

Quantifying landscape change in an arctic coastal lowland using repeat airborne LiDAR

Benjamin M Jones^{1,7}, Jason M Stoker², Ann E Gibbs³, Guido Grosse⁴, Vladimir E Romanovsky⁴, Thomas A Douglas⁵, Nicole E M Kinsman⁶ and Bruce M Richmond³

¹ Alaska Science Center, US Geological Survey, Anchorage, AK 99508, USA

² Earth Resource and Observation Science Center, US Geological Survey, Sioux Falls, SD 57198, USA

³ Pacific Coastal and Marine Science Center, US Geological Survey, Santa Cruz, CA 95060, USA

⁴ Geophysical Institute, University of Alaska Fairbanks, Fairbanks, AK 99775, USA

⁵ US Army Cold Regions Research and Engineering Laboratory, Fort Wainwright, AK 99703, USA

⁶ Alaska Division of Geological and Geophysical Surveys, Fairbanks, AK 99708, USA

E-mail: bjones@usgs.gov

Received 5 June 2013

Accepted for publication 21 October 2013

Published 21 November 2013

Online at stacks.iop.org/ERL/8/045025

Abstract

Increases in air, permafrost, and sea surface temperature, loss of sea ice, the potential for increased wave energy, and higher river discharge may all be interacting to escalate erosion of arctic coastal lowland landscapes. Here we use airborne light detection and ranging (LiDAR) data acquired in 2006 and 2010 to detect landscape change in a 100 km² study area on the Beaufort Sea coastal plain of northern Alaska. We detected statistically significant change (99% confidence interval), defined as contiguous areas (>10 m²) that had changed in height by at least 0.55 m, in 0.3% of the study region. Erosional features indicative of ice-rich permafrost degradation were associated with ice-bonded coastal, river, and lake bluffs, frost mounds, ice wedges, and thermo-erosional gullies. These features accounted for about half of the area where vertical change was detected. Inferred thermo-denudation and thermo-abrasion of coastal and river bluffs likely accounted for the dominant permafrost-related degradational processes with respect to area (42%) and volume (51%). More than 300 thermokarst pits significantly subsided during the study period, likely as a result of storm surge flooding of low-lying tundra (<1.4 m asl) as well as the lasting impact of warm summers in the late-1980s and mid-1990s. Our results indicate that repeat airborne LiDAR can be used to detect landscape change in arctic coastal lowland regions at large spatial scales over sub-decadal time periods.

Keywords: Arctic, coasts, LiDAR, permafrost, thermokarst

1. Introduction

Recent reductions in Arctic sea ice extent have been well documented (Stroeve *et al* 2012). Reduced sea ice cover, combined with earlier seasonal thaw and later winter

freeze-up results in increased effective fetch for wind-wave generation and a longer time period of open water for storms to impact arctic coastal lowlands (Overeem *et al* 2011). Increases in river discharge may also be enhancing erosion along riverine corridors, although pan-Arctic evaluations of river discharge reveal contrasting regional trends (McClelland *et al* 2006). In addition, warming of terrestrial permafrost (Romanovsky *et al* 2010, Smith *et al* 2010) may lead to thermokarst development and other thaw-related phenomena in ice-rich permafrost terrain (Jorgenson *et al* 2006).



Content from this work may be used under the terms of the [Creative Commons Attribution 3.0 licence](http://creativecommons.org/licenses/by/3.0/). Any further distribution of this work must maintain attribution to the author(s) and the title of the work, journal citation and DOI.

⁷ Author to whom any correspondence should be addressed.

Thus, terrestrial, aquatic, and marine environmental changes occurring in the Arctic may be interacting to increase erosion of coastal lowland landscapes which in turn may lead to mobilization of carbon previously frozen in permafrost (Jorgenson and Brown 2005, Lantuit *et al* 2009).

Thus far, most remote sensing studies focused on identifying landscape change of near surface permafrost terrain in arctic lowland regions primarily rely on two-dimensional measurements to quantify lateral rates of change for thermokarst lakes (Arp *et al* 2011, Jones *et al* 2011), thermokarst lake drainage (Hinkel *et al* 2007, Marsh *et al* 2009), retrogressive thaw slump headwall retreat (Lantz and Kokelj 2008, Lantuit and Pollard 2008), thermo-erosional gully formation and expansion (Fortier *et al* 2007), erosion of coasts by block collapse and mass wasting (Jones *et al* 2009), and degradation of ice wedges and thermokarst pit formation (Jorgenson *et al* 2006). A few remote sensing studies in lowland permafrost terrain have targeted three-dimensional landscape change relying on Interferometric Synthetic Aperture Radar (InSAR) techniques (e.g. Liu *et al* 2010). While InSAR is capable of capturing broad regional dynamics of land surface heave and subsidence the method is limited in its applicability for detecting thermokarst features (Short *et al* 2011). In addition, stereo-photogrammetric change detection studies have been limited in nature and spatial extent in lowland permafrost regions (Lantuit and Pollard 2005, Günther *et al* 2013), whereas their use is more widespread in mountainous permafrost regions (e.g. Kääh 2008).

The ability to detect vertical change in permafrost regions is critical to advancing our understanding of landscape evolution and carbon cycling. Light detection and ranging (LiDAR) measurements provide a powerful method for imaging the spatial and vertical intricacies of the landscape (e.g. Ritchie 1995). Successful applications of airborne LiDAR include the study of stream morphology (e.g. Snyder 2009), mapping coastline morphologic change (e.g. White and Wang 2003), measuring volumetric change in sand dunes (e.g. Woolard and Colby 2002), landslide monitoring (e.g. Glenn *et al* 2006), and topographic change of periglacial mountainous terrain (Fischer *et al* 2011). However, airborne LiDAR data has seldom been used to characterize periglacial lowland regions (Marsh *et al* 2009, Hubbard *et al* 2013). To date, an airborne LiDAR change detection study for coastal lowland permafrost terrain has not been attempted to the best of our knowledge.

In this study, we contrast airborne LiDAR data collected in July 2006 and July 2010 for a 100 km² area on the central Beaufort Sea coastal plain in northern Alaska. We use repeat LiDAR to test whether this approach is capable of detecting geomorphic changes occurring in arctic coastal lowland landscapes, particularly those associated with thermokarst and other thaw-related processes. We also present trends in mean annual air temperature, thawing degree days (TDD), near surface permafrost temperature, and active layer thickness for monitoring sites in close proximity to our study region. In addition, we provide an example of how repeat LiDAR data may be used regarding questions of

carbon mobilization from permafrost terrain. These inquiries align with the increasing interest in the spatial and temporal dynamics of permafrost-dominated landscapes from a wide range of science and engineering disciplines (landscape ecology, hydrology, civil engineering, and biogeochemistry) and will be helpful in addressing land management issues such as infrastructure planning, habitat mapping, and landscape evolution in the Arctic.

2. Study area

The study area is located on the Beaufort Sea coastal plain of northern Alaska and was selected due to existing, overlapping coverage of airborne LiDAR data acquired in July 2006 and July 2010. Repeat LiDAR data were available for a nearly 100 km² land area along the coast from the Sagavanirktok River delta in the west to Point Thomson in the east, with an inland coverage of 2–4 km (figure 1). The study region contains thermokarst and other thaw-related landscape features as well as nearshore coastal and fluvial morphology (figure 2). The backshore lithology consists of ice cemented, pebbly silty sand, with 70–80% volumetric ground ice content, and 10–20% by volume of ice-wedge ice (Jorgenson and Brown 2005, Kanevskiy *et al* 2013). Sea ice, predominantly landfast ice, is typically present along the coast for 8–9 months of the year. The astronomical tides in this region are typically less than 0.2 m, however, atmospheric and oceanic conditions have led to storm surges as high as 1.4 m above mean sea level during the last two decades (Sultan *et al* 2011). Long-term mean annual coastal erosion rates in our study region are 0.9 m yr⁻¹ and maximum observed rates are 7.0 m yr⁻¹ (Jorgenson and Brown 2005, Gibbs *et al* 2011), and there has been a doubling of the mean decadal-scale coastal erosion rate since the 1980s (Ping *et al* 2011). Estimates of total organic carbon (OC) in the upper 1 m of the landscape range from 56 to 66 kgOC m⁻² at particular sample sites (Ping *et al* 2008) and estimates of carbon mobilization in our study area as a result of coastal erosion range from 3.2 to 7.1 Gg yr⁻¹ (Jorgenson and Brown 2005).

The study area also encompasses existing and planned oil and gas infrastructure. Development within the study area primarily consists of commercial resource extraction and resource transportation infrastructure emplaced by the oil and gas industries (e.g. drilling pads, pipelines, airstrips and docks). There are approximately eight known exploratory or production well sites within the bounds of the study area, the largest being the Badami oil field. Standard construction methods for development in this area utilize gravel pads to thermally buffer the underlying permafrost. These gravel features provide an excellent location for validating the comparability in the two LiDAR datasets as their vertical motion should be near zero (figure 3).

3. Methods

3.1. Airborne LiDAR data

LiDAR was collected in the summers of 2006 and 2010 by Aero-metric Inc. The 2006 data were delivered as classified

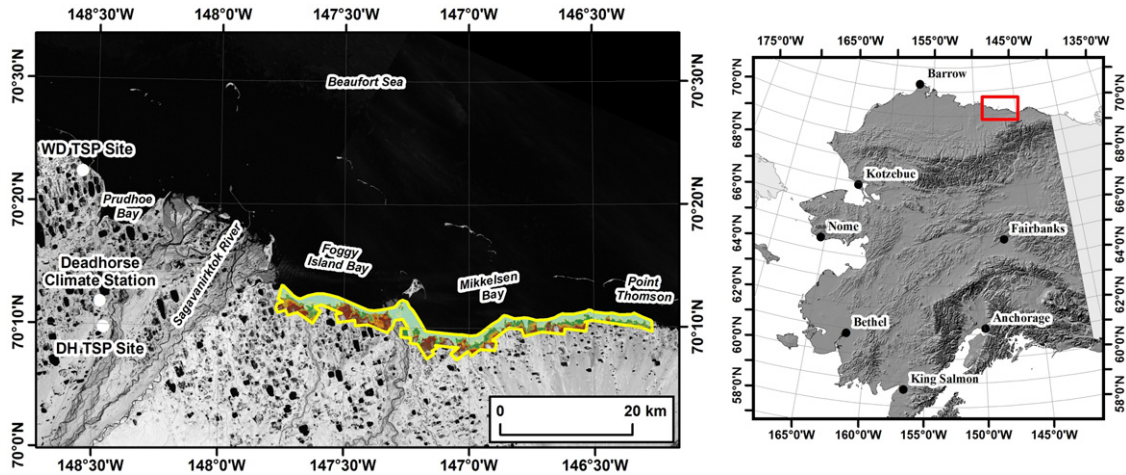


Figure 1. The 100 km² repeat LiDAR study area on the central Beaufort Sea coastal plain is outlined with the yellow polygon. The background image is a 30 m resolution Landsat image. The climate station is the location of observations on mean annual air temperature and thawing degree day sums. The West Dock (WD) and Deadhorse (DH) Thermal State of Permafrost (TSP) observatories are the location of ground temperature data and active layer thickness measurements used in this study. The location of the study region (red box) in Alaska is shown in the map on the right.

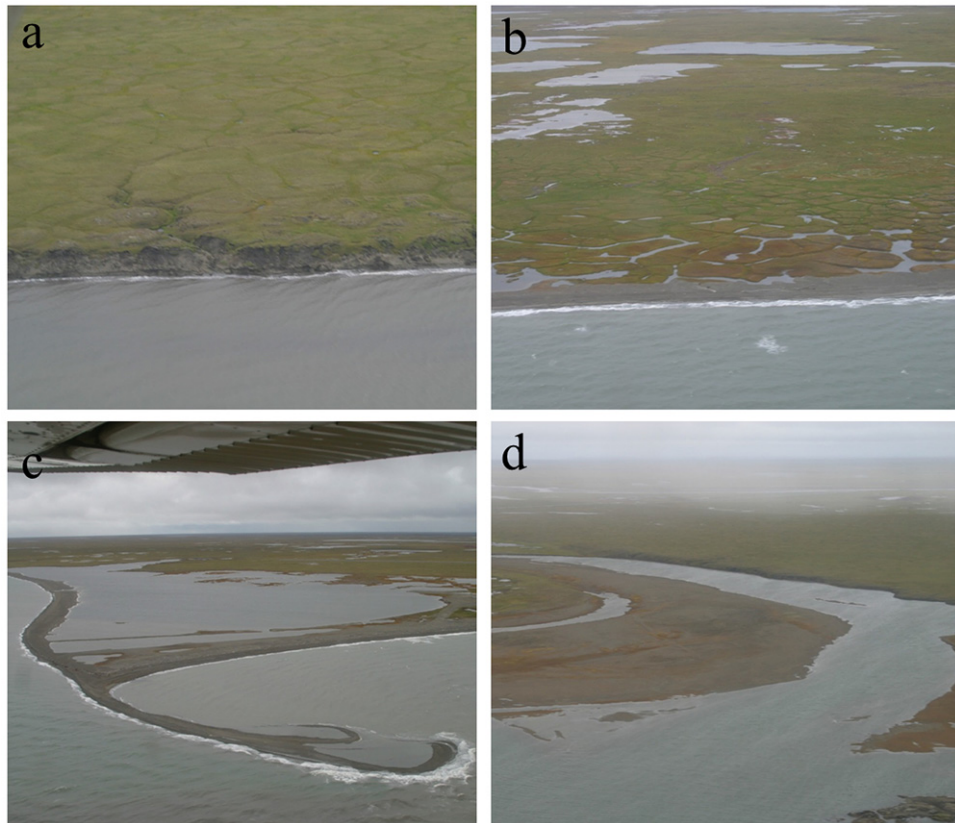


Figure 2. Oblique photos from the study region acquired in 2006 showing the coastal setting and hinterland features (Gibbs and Richmond 2009). (a) A coastal bluff showing a thermo-erosional gully, thermo-denudation, and ice-wedge polygons; (b) a coastal lowland setting showing degraded ice wedges, thermokarst ponds, and beach deposits; (c) spit and beach features enclosing a shallow lagoon; and (d) a low gradient river channel, river bar, and cut bank.

point clouds in NAD 83 Alaska State Plane Zone 3 in feet, with elevations referenced to Geoid99 in US Survey feet. The 2010 data were delivered as last return point clouds in NAD 83 UTM zone 6N in meters, with elevations referenced to

the GRS 1980 Ellipsoid. The 2006 data were transformed to match the horizontal and vertical units and Ellipsoid reference frame of the 2010 data. Nominal point spacing for the data was on average one point per 1–1.5 m for both datasets.

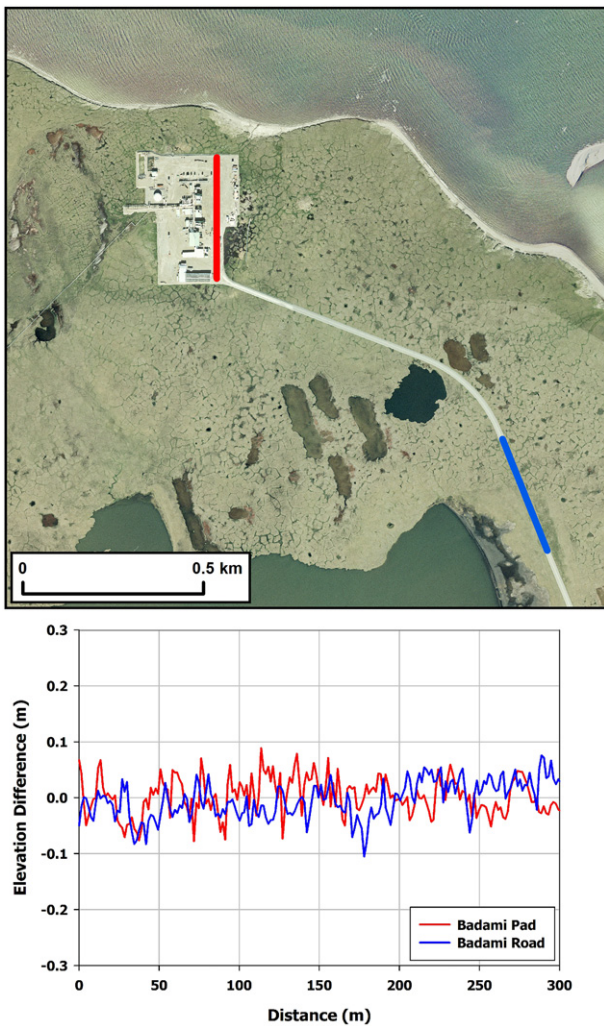


Figure 3. Detailed comparison between the 2006 and 2010 LiDAR datasets for presumed vertically stable features on an unvegetated land surface in the study area. The Badami oil field pad and road show that the difference in elevation between the two datasets is on the order of ± 0.1 m.

Both last return, point cloud datasets were clipped to their overlapping extents, and then converted to surfaces, first by using Terrascan (version 12)[®] and a Triangulated Irregular Network (TIN) approach. The TIN connects LiDAR returns by a set of contiguous, non-overlapping, Delaunay triangles. The elevations between each triangle vertex are interpolated as definitions of planes and thus together construct a surface. These surfaces were then exported to lattice datasets, and finally converted to 1.5 m raster grids to be used in a GIS.

The two datasets were differenced to identify potential changes in elevation between 2006 and 2010. The reported vertical accuracies of the data were 0.12 m (2006 dataset) and 0.14 m (2010 dataset) RMSE. To determine if there were any errors introduced in the conversion/transformation process we compared elevations along transects that likely represented stable terrain features associated with oil infrastructure gravel pads between the two acquisition dates. The difference in elevation along the unvegetated land surfaces were less than ± 0.10 m (figure 3). However to be conservative in our

detection of change, and with the realization that comparison of the data acquired over gravel pads represent a best case scenario, we used the RMSE of the individual datasets to calculate (equation (1)) a threshold that describes the minimum difference between both datasets that meets a significant elevation change at the 99% confidence level or those pixels exceeding three standard deviations (Jaw 2001):

$$3\text{SQRT} \left((2006 \text{ vertical accuracy})^2 + (2010 \text{ vertical accuracy})^2 \right) = 0.55 \text{ m.} \quad (1)$$

In the surface differenced raster, we considered any pixel with a height difference residual above or below 0.55 m as a statistically significant change in elevation. These areas were reclassified as (significant increase) or (significant decrease) per pixel. Objects demonstrating significant increases or decreases in elevation were extracted from the dataset by selecting areas that had at least five contiguous pixels of significant change. This resulted in a minimum object size greater than 10 m² and helped minimize potential errors associated with raster grid creation and horizontal positional accuracy (± 0.60 m). While there were detectable changes of smaller amplitude in the difference image we did not consider these in our further assessment. In addition, all changes interpreted as indicating water level differences as well as a result of human-caused landscape changes, such as from infrastructure construction or material movement, were excluded from further analysis.

3.2. Geomorphic classification of landscape change units

Objects that represented a statistically significant change in elevation were manually classified as one of 13 categories via visual inspection of the LiDAR imagery. Nine of these classes represented land subsidence or loss and four represented land uplift or deposition. Objects that were indicative of subsidence included thermokarst and thaw-related features associated with ice-bonded coastal, river, and lake bluffs, frost mounds, ice wedges, and thermo-erosional gullies. Non-thaw-related erosional features included beaches and spits, river bars and deltas, and sand dunes. Areas that represented landscape uplift or deposition included permafrost heave features and deposition associated with beaches and spits, river bars and deltas, and sand dunes (often in close proximity to an eroding feature).

3.3. Air and permafrost temperature and active layer thickness measurements

The West Dock (WD) and Deadhorse (DH) Thermal State of Permafrost (TSP) permafrost observatories were established in the late 1970s (Osterkamp 2003). The WD TSP site is located 0.3–0.4 km from the coast and the DH TSP site is located 15 km from the coast (figure 1). Vegetation at each site consists of wet non-acidic tundra with a continuous cover of graminoid and moss species and wet and moist non-acidic tundra composed of graminoid–moss tundra and graminoid, prostrate-dwarf-shrub, moss tundra, respectively (Walker *et al*

Table 1. Classified change objects in the repeat LIDAR study area. The table provides information on the type of feature, the number of discrete polygons greater than 10 m², the minimum, maximum, mean, and sum for 2D and 3D changes, and the rate of change in 2D and 3D space.

Feature type	Number	Area (m ²)				Vertical change (m)				Change rate	
		Minimum	Maximum	Mean	Sum	Minimum	Maximum	Mean	Sum	Area (m ² yr ⁻¹)	Volume (m ³ yr ⁻¹)
Coastal bluff erosion	341	11	20 115	360	123 020	0.6	4.4	0.8	60 541	30 755	1861 938 455
River bluff erosion	113	11	648	61	6 903	0.6	3.8	0.8	2 780	1 726	4 797 585
Thaw slump	24	11	266	48	1 161	0.7	1.6	0.8	452	290	131 193
Thermokarst lake Erosion	15	11	884	115	1 725	0.7	2.4	0.9	889	431	383 381
Thermokarst pit	344	11	70	18	6 237	0.6	1.0	0.7	1 872	1 559	2 918 916
Thermo-erosional gully	43	11	250	29	1229.1	0.7	1.8	0.7	407	307	125 061
Heave features	42	11	131	25	1 064	0.6	1.4	0.8	388	266	103 208
Beach/spit erosion	451	11	11 724	295	133 112	0.6	2.6	0.7	51 988	33 278	1730 056 664
Delta/river bar erosion	124	11	693	55	6 846	0.6	1.3	0.7	2 178	1 712	3 727 647
Dune erosion	20	11	72	26	528	0.6	0.9	0.7	159	132	20 988
Beach/spit deposition	194	11	2 218	129	25 148	0.6	1.6	0.7	8 568	6 287	53 867 016
Delta/river bar deposition	3	11	171	70	209	0.6	1.0	0.8	67.5	52	3 527
Dune deposition	4	11	52	22	88	0.6	1.3	0.8	32	22	704

2008). In 1986, a string of calibrated thermistors attached to a data logger were installed at each site (Osterkamp 2003, Romanovsky and Osterkamp 1995). In 1997, the measuring systems at each site were upgraded with new calibrated thermistor strings (MRC thermistor string) and Campbell Scientific data loggers (Romanovsky *et al* 2003). The old and new measuring systems were run concurrently for two years and differences in the temperature readings obtained from the two measuring systems at the same depth were typically within 0.2 °C. Mean annual ground temperature at a depth of 70 cm for the time period of 1987–2010 was calculated using the daily averaged records from the WD and DH TSP sites. In 1996, a one hectare grid was established at each permafrost observatory to measure active layer thickness. Measurements were conducted every 10 m in accordance with the Circumpolar Active Layer Monitoring (CALM) program protocol (Brown *et al* 2000). To derive mean annual air temperature trends and TDD (based on 0 °C) we used data from the Deadhorse airport climate station (figure 1). This station has been in operation since 1973, however due to data continuity issues we only present data for the period 1983–2010. These two permafrost monitoring sites and the climate station are considered representative of conditions within the repeat LiDAR study area.

4. Results

Comparison between the 2006 and 2010 LiDAR datasets revealed that 0.3% (by area) of the landscape experienced a statistically significant change in elevation (>0.55 m) over the four year period. A total of 1718 discrete objects (>10 m²) with significant change were identified. Changes

in elevation were classified by geomorphic unit where the most likely mechanism of change was inferred to be: thaw slumping (figure 4(a)), coastal bluff erosion (figure 4(b)), river bluff erosion, thermokarst lake expansion, thermokarst pit subsidence (figure 4(c)), thermo-erosional gully erosion, permafrost heave, beach/spit erosion/deposition, delta/river bar erosion/deposition, and sand dune erosion/deposition (table 1). Coastal bluff erosion, thermokarst pit subsidence, and beach/spit erosion accounted for 66% of the identified objects. Thaw slumps, thermokarst lake expansion, river bluff erosion, thermo-erosional gullies, delta/river bar erosion, and sand dune blowouts accounted for the remainder of the land lowering/loss. Beach/spit deposition accounted for 82% of the significant increase in surface elevation; whereas heave features, delta/river bar deposition, and sand dune accumulation accounted for the remainder of the detectable increase in the land surface elevation.

The largest individual, contiguous erosional objects by mean area were coastal bluffs (360 m²), beaches/spits (295 m²), and expanding thermokarst lake margins (115 m²). All other erosional and depositional objects had a mean surface area of less than 100 m². Coastal bluff erosion accounted for 40% of the total area where elevation changes were observed and beach spit erosion accounted for 43%. Thermokarst pit subsidence, river bluff erosion, and delta/river bar erosion each accounted for 2% of the area with observed elevation change. All other erosional features accounted for less than 1% of the total detectable surface area change. In terms of vertical change, coastal bluffs (4.4 m), river bluffs (3.8 m), beaches/spits (2.6 m), and thermokarst lake bluffs (2.4 m) accounted for objects with the greatest maximum change in elevation. Volumetrically, coastal bluff

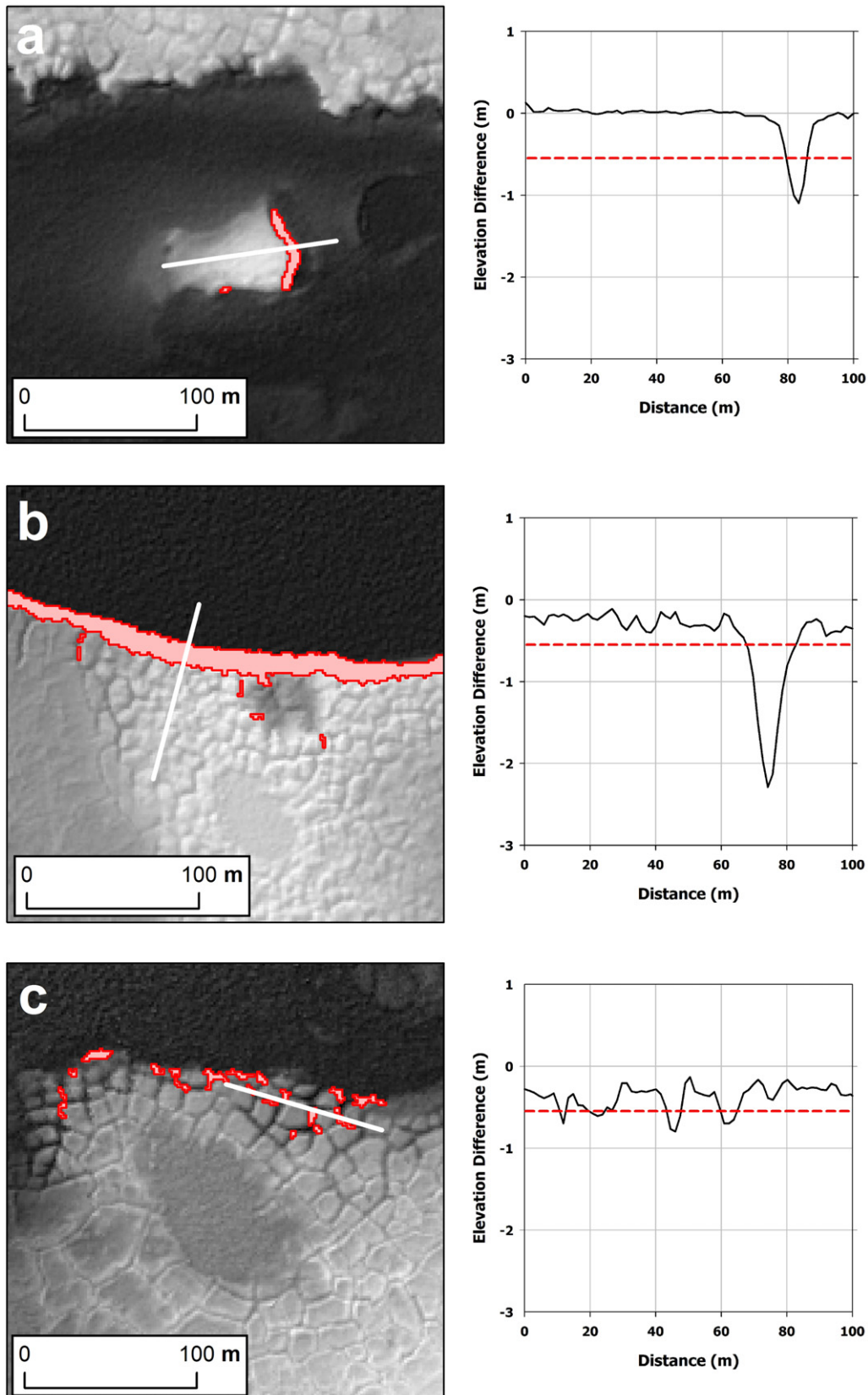


Figure 4. Example of change detection results from the repeat LiDAR datasets showing a hillshade image on the left and elevation difference profiles on the right. The red polygons on the left indicate significant change objects as do the segments of the elevation difference profiles (taken from transects marked with white line on left) below the red dashed line. (a) Degradation of a frost mound in a drained thermokarst lake basin. Note the excellent agreement between the 2006 and 2010 profiles. (b) Erosion along a 4 m high coastal bluff. Thermokarst gully and thermokarst pit formation are also evident (similar to the setting in figure 2(a)). (c) Thermokarst pit formation in coastal lowland (similar to the setting in figure 2(b)). Note general lowering of the land surface in examples (b) and (c).

erosion accounted for 51% and beach/spit erosion 47% of the detectable changes. Beach/spit deposition accounted for 1.5% and all other features were equal to or less than 0.1% of the volume change.

5. Discussion

5.1. Airborne LiDAR change detection

Our results indicate that repeat airborne LiDAR measurements provide a straightforward, readily applied tool for quantifying landscape change in arctic coastal lowland regions. Comparison of the two LiDAR datasets revealed that 0.3% of the landscape area experienced a significant change in elevation between 2006 and 2010 that resulted from thaw and non-thaw-related processes. Thermokarst or thaw-related landscape features associated with ice-bonded coastal, river, and lake bluffs, thermokarst pits, thaw slumps, and thermo-erosional gullies accounted for 46% of the change in area over the four year study period and more than half of the significant change (56%) resulted from erosion and deposition associated with beach and spit deposits, riverine and deltaic flats, and sand dunes. These short-term landscape dynamics are likely a result of a combination of factors related to both natural processes and changes in the terrestrial, aquatic, and marine controls on the region.

Detailed examples of features detected in the study area include frost mound degradation (figure 4(a)); coastal bluff erosion, thermo-erosional gully expansion, and upland ice-wedge degradation (figure 4(b)); and lowland ice wedge degradation and thaw pit formation (figure 4(c)). Comparison between the 2006 and 2010 LiDAR data for the frost mound shows the excellent agreement (typically ± 0.15 m) between the two datasets for a vegetated and sloping surface that experienced a minimal change in height. Degradation or slumping of the eastern margin of the feature accounted for quantifiable change. In the example given in figure 4(b), the ~ 4 m high bluff-face migrated 13 m inland over the four year study period. Also, evident in this example is an overall lower tundra relief in 2010 compared to 2006. Tundra lowering in this example did not meet our minimum threshold for change detection however, a consistent decrease in the elevation is visible in the plotted data that could be a result of top down permafrost thaw and soil consolidation. This general pattern of tundra relief lowering is also evident in figure 4(c) for which we also detected a number of degrading ice wedges. The changes evident in this example may be a result of frequent inundation of the terrain during storm surges (Sultan *et al* 2011) which may lead to degradation of the ice-rich permafrost and degradation of ice wedges (figure 2(b)). With more local ground control statistically significant changes in elevation could be refined to capture these more subtle surface changes.

5.2. Factors contributing to landscape change

Arctic coastal lowland regions are particularly vulnerable to change given the interaction of atmospheric, terrestrial,

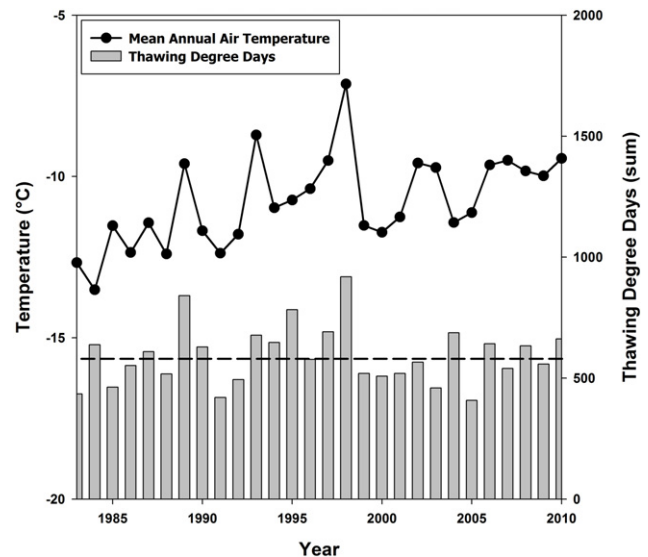


Figure 5. Mean annual air temperature and summertime (June–September) thawing degree day sums from 1983 to 2010 for the Deadhorse, AK climate station (NCDC 2013). The dashed line indicates the mean value for TDD over the period of observation.

aquatic, and marine influences on landscape configuration. Thermokarst and other thaw-related landscape features are driven by either local or regional disturbances. Jorgenson *et al* (2006) noted an abrupt increase in ice-wedge degradation and thermokarst pit formation on the Beaufort Sea coastal plain that was attributed to an increase in TDD in the late-1980s and throughout the 1990s. A compilation of TDD from 1983 to 2010 for the Deadhorse climate station shows that the TDD in 2006, 2008, and 2010 exceeded the ~ 30 year average (figure 5). In addition, the 2006–2010 time period experienced some of the highest combined, continuous mean annual and mean summer temperatures over the course of the record for the Deadhorse climate station. No individual year rivaled the number of TDD that occurred in 1989, 1995, or 1998, which Jorgenson *et al* (2006) attributed to the widespread formation of thermokarst pits. It should be noted however that the warm summers in the late-1980s and mid-1990s could also be responsible for some of the observed increase in pit formation in our study region between 2006 and 2010, as the thermokarst pits that likely formed during the 1990s have continued to subside. A recent analysis of thermokarst pit formation over a 60 year period in the Prudhoe Bay oil fields indeed shows a substantial increase in thermokarst pit formation between 1990 and 2001 that has continued through 2010 (Raynolds *et al* 2013).

Mean annual air temperature and the temperature of the ground as measured at a depth of 70 cm have warmed in the study region during the past ~ 20 to ~ 30 years, respectively (figures 5 and 6(a)). Interestingly, there is a mismatch between these warming trends and the trend in active layer thickness (figure 6(b)). This lack of coherence may be explained by the thaw of ice-rich permafrost and settlement of the ground surface as excess ice melts and the soil consolidates. Liu *et al* (2010) measured ground deformation using InSAR from 1992 to 2000 in this region and found that seasonal vertical

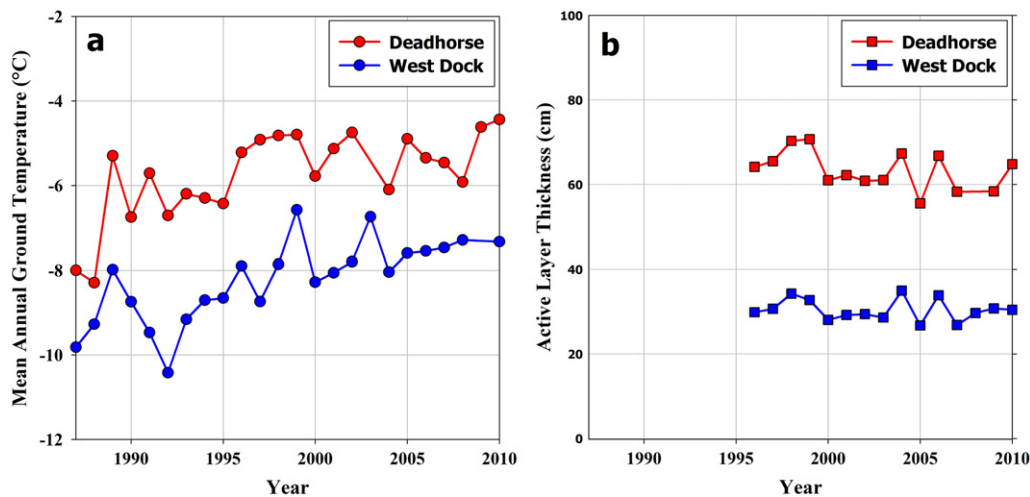


Figure 6. (a) Near surface permafrost temperature data measured at a depth of 70 cm and (b) active layer thickness measurements from the Deadhorse (DH) and West Dock (WD) Thermal State of Permafrost (TSP) sites between 1987 and 2010 and 1996 and 2010, respectively.

displacements occurred as a result of freezing and thawing of the ground surface but that there was a secular subsidence of the land surface on the order of 1–4 cm/decade. Ground based studies on the Beaufort Coastal Plain from 2001 to 2006 indicate that $>2.0 \text{ cm yr}^{-1}$ of subsidence occurred and that when combined with mechanical probing measurements of the active layer that there was an increase in the ‘true’ thaw depth (Streletskiy *et al* 2008). Thus, while general ground subsidence was not detected due to our conservative measure of change some of the lowering of the landscape observed in the data outside our defined level of confidence may indeed be a result of top down permafrost thaw.

The Alaskan Beaufort Sea coast has experienced varying levels of increased rates of erosion since the 1950s (Jones *et al* 2009, Gibbs *et al* 2011, Ping *et al* 2011). Factors responsible for this likely include loss of sea ice, warming ocean temperatures, and an increase in total wave energy (Overeem *et al* 2011). While no comprehensive studies on river discharge or river bluff erosion exist in the study region, Arctic wide assessments indicate varying degrees of changes to river discharge (McClelland *et al* 2006) which may be impacting erosion of river bluffs. These changes are likely interacting to increase the effectiveness of thermal erosion and thermal abrasion of coastal and river bluffs in our study area. These processes likely accounted for the dominant permafrost-related degradational processes with respect to area (42%) and volume (51%) in the study region. In addition, areas lower than 1.4 m relative to mean sea level have been inundated during storm surges over the past two decades (Sultan *et al* 2011). Two of the ten highest storm surges between 1993 and 2010 occurred during our study period and all but one occurred between 2000 and 2010. Inundation of the low-lying coastal zone in our study area has likely contributed to the formation of thermokarst pits, with 60% of the observed change associated with these features below this approximate elevation (figure 4(c)). These inundation events may have also contributed to some of the general land lowering along the low-lying coastal zone that was observed in the data but outside our defined level of confidence.

5.3. Organic carbon mobilization

Estimates of total organic carbon in the upper 1 m of the studied landscape range from 56 to 66 kg OC m^{-2} at sample sites located in the study region (Ping *et al* 2008). Based on these estimates, the loss of land between 2006 and 2010 along coast and river bluffs may have mobilized 1.8–2.1 Gg yr^{-1} . However, given our conservative estimates of quantifiable change this number should be viewed as a minimum estimate since long-term estimates of carbon flux from this coastal stretch range from 3.0 to 7.0 Gg yr^{-1} (Jorgenson and Brown 2005). This exercise simply illustrates a basic type of analysis for carbon-related studies in permafrost terrain where repeat airborne LiDAR surveys have been acquired.

6. Conclusion

We compared airborne LiDAR data from 2006 and 2010 and demonstrated that it is possible to detect and characterize a number of thaw-related and non-thaw-related landscape changes occurring in arctic coastal lowlands. Erosion of ice-bonded coastal and river bluffs, thaw slumping, thermokarst lake expansion, thermokarst pit subsidence, and thermo-erosional gully expansion indicated ice-rich permafrost degradation and accounted for nearly half of the area and half of the volume change that occurred over the four year study period. Erosion and deposition associated with beach and spit deposits, riverine and deltaic flats, and sand dunes accounted for the majority of the remaining significant landscape change. Our study demonstrates the utility of assessing landscape change in an arctic coastal lowland with repeat airborne LiDAR data, in particular for spatially small but widespread permafrost thaw-related processes. We hope that this study will encourage the collection of repeat LiDAR data in other permafrost terrain.

Acknowledgments

Funding for this research was primarily provided by the US Geological Survey—Alaska Regional Directors Office,

Alaska Science Center, the Earth Resource and Observation Science Center, the National Geospatial Program, and the Coastal and Marine Geology Program. Additional support was provided by the Arctic Landscape Conservation Cooperative and GG was supported by NASA grant #NNX08AJ37G. TAD was supported by funding from the Strategic Environmental Research and Development Program (SERDP) Project RC-2110. We kindly thank Stephan Gruber, Carl Markon, and an anonymous reviewer for their thoughtful and thorough critique of this letter. Any use of trade, product, or firm names is for descriptive purposes only and does not imply endorsement by the US Government.

References

- Arp C D, Jones B M, Urban F E and Grosse G 2011 Hydrogeomorphic processes of thermokarst lakes with grounded ice and floating ice regimes on the Arctic coastal plain, Alaska *Hydrol. Process.* **25** 2422–38
- Brown J, Hinkel K M and Nelson F E 2000 The Circumpolar Active Layer Monitoring (CALM) program: research designs and initial results *Polar Geogr.* **24** 163–258
- Fischer L, Eisenbeiss H, Kääb A, Huggel C and Haerberli W 2011 Monitoring topographic changes in a periglacial high-mountain face using high-resolution DTMs, Monte Rosa East Face, Italian Alps *Permafrost Periglac. Process.* **22** 140–52
- Fortier D, Allard M and Shur Y 2007 Observation of rapid drainage system development by thermal erosion of ice wedges on Bylot Island, Canadian Arctic Archipelago *Permafrost Periglac. Process.* **18** 229–43
- Gibbs A E, Harden E L, Richmond B M and Erikson L H 2011 Regional shoreline change and coastal erosion hazards in Arctic Alaska *Proc. Solutions to Coastal Disasters Conf. ASCE* ed L A Wallendorf, C Jones, L Ewing and B Battalio, pp 258–72
- Gibbs A E and Richmond B M 2009 Oblique aerial photography of the Arctic coast of Alaska, Nulavik to Demarcation Point, August 7–10 2006 *US Geological Survey Data Series 436* <http://pubs.usgs.gov/ds/436/>
- Glenn N F, Streutker D R, Chadwick D J, Thackray G D and Dorsch S J 2006 Analysis of LiDAR-derived topographic information for characterizing and differentiating landslide morphology and activity *Geomorphology* **73** 131–48
- Günther F, Overduin P P, Baranskaya A, Opel T and Grigoriev M N 2013 Observing muostakh Island disappear: erosion of a ground-ice-rich coast in response to summer warming and sea ice reduction on the east Siberian shelf *Cryosphere Discuss.* **7** 4101–76
- Hinkel K M, Jones B M, Eisner W R, Cuomo C J, Beck R A and Frohn R 2007 Methods to assess natural and anthropogenic thaw lake drainage on the western Arctic coastal plain of northern Alaska *J. Geophys. Res.* **112** F02S16
- Hubbard S S *et al* 2013 Quantifying and relating land-surface and subsurface variability in permafrost environments using LiDAR and surface geophysical datasets *Hydrogeol. J.* **21** 149–69
- Jaw J 2001 Statistics-based fusion of terrain data sets and change detection *Proc. 22nd Asian Conf. on Remote Sensing (Singapore, Nov. 2001)* Centre for Remote Imaging, Sensing and Processing, National University of Singapore p 6 www.crisp.nus.edu.sg/~acrs2001/pdf/278JAW.pdf
- Jones B M, Arp C D, Jorgenson M T, Hinkel K M, Schmutz J A and Flint P L 2009 Increase in the rate and uniformity of coastline erosion in Arctic Alaska *Geophys. Res. Lett.* **36** L03503
- Jones B M, Grosse G, Arp C D, Jones M C, Anthony K W and Romanovsky V E 2011 Modern thermokarst lake dynamics in the continuous permafrost zone, northern Seward Peninsula, Alaska *J. Geophys. Res.* **116** G00M03
- Jorgenson M T and Brown J 2005 Classification of the Alaskan Beaufort Sea Coast and estimation of carbon and sediment inputs from coastal erosion *Geo-Mar. Lett.* **25** 69–80
- Jorgenson M T, Shur Y L and Pullman E R 2006 Abrupt increase in permafrost degradation in Arctic Alaska *Geophys. Res. Lett.* **33** L02503
- Kääb A 2008 Remote sensing of permafrost-related problems and hazards *Permafrost Periglac. Process.* **19** 107–36
- Kanevskiy M *et al* 2013 Ground ice in the upper permafrost of the Beaufort Sea coast of Alaska *Cold Reg. Sci. Technol.* **85** 56–70
- Lantuit H and Pollard W H 2005 Temporal stereophotogrammetric analysis of retrogressive thaw slumps on Herschel Island, Yukon Territory *Nat. Hazards Earth Syst. Sci.* **5** 413–23
- Lantuit H and Pollard W H 2008 Fifty years of coastal erosion and retrogressive thaw slump activity on Herschel Island, southern Beaufort Sea, Yukon Territory, Canada *Geomorphology* **95** 84–102
- Lantuit H, Rachold V, Pollard W H, Steenhuisen F, Ødegård R and Hubberten H W 2009 Towards a calculation of organic carbon release from erosion of Arctic coasts using non-fractal coastline datasets *Mar. Geol.* **257** 1–10
- Lantz T C and Kokelj S V 2008 Increasing rates of retrogressive thaw slump activity in the Mackenzie Delta region, NWT, Canada *Geophys. Res. Lett.* **35** L06502
- Liu L, Zhang T and Wahr J 2010 InSAR measurements of surface deformation over permafrost on the North Slope of Alaska *J. Geophys. Res.* **115** F03023
- Marsh P, Russell M, Pohl S, Haywood H and Onclin C 2009 Changes in thaw lake drainage in the Western Canadian Arctic from 1950 to 2000 *Hydrol. Process.* **23** 145–58
- McClelland J W, Déry S J, Peterson B J, Holmes R M and Wood E F 2006 A pan-arctic evaluation of changes in river discharge during the latter half of the 20th century *Geophys. Res. Lett.* **33** L06715
- NCDC (National Climate Data Center) 2013 www.ncdc.noaa.gov/cdo-web/
- Osterkamp T E 2003 Establishing long-term permafrost observatories for active layer and permafrost investigations in Alaska: 1977–2002 *Permafrost Periglac. Process.* **14** 331–42
- Overeem I, Anderson R S, Wobus C W, Clow G D, Urban F E and Matell N 2011 Sea ice loss enhances wave action at the Arctic coast *Geophys. Res. Lett.* **38** L17503
- Ping C L, Michaelson G J, Jorgenson M T, Kimble J M, Epstein H, Romanovsky V E and Walker D A 2008 High stocks of soil organic carbon in the North American Arctic region *Nature Geosci.* **1** 615–9
- Ping C L *et al* 2011 Soil carbon and material fluxes across the eroding Alaska Beaufort Sea coastline *J. Geophys. Res.* **116** G02004
- Raynolds M K *et al* 2013 Cumulative effects of 62 years of infrastructure and climate change in ice-rich permafrost landscapes, Prudhoe Bay Oilfield, Alaska *Proc. Natl Acad. Sci.* in review, submitted
- Ritchie J C 1995 Airborne laser altimeter measurements of landscape topography *Remote Sens. Environ.* **53** 91–6
- Romanovsky V E and Osterkamp T E 1995 Interannual variations of the thermal regime of the active layer and near-surface permafrost in Northern Alaska *Permafrost Periglac. Process.* **6** 313–35
- Romanovsky V E, Sergueev D O and Osterkamp T E 2003 Temporal variations in the active layer and near-surface permafrost temperatures at the long-term observatories in Northern Alaska *Eighth Int. Conf. on Permafrost* ed M Phillips, S Springman and L U Arenson (Lisse: Swets & Zeitlinger) pp 989–94
- Romanovsky V E, Smith S L and Christiansen H H 2010 Permafrost thermal state in the polar Northern Hemisphere during the

- international polar year 2007–2009: a synthesis *Permafrost Periglac. Process.* **21** 106–16
- Short N, Brisco B, Couture N, Pollard W, Murnaghan K and Budkewitsch P 2011 A comparison of TerraSAR-X, RADARSAT-2 and ALOS-PALSAR interferometry for monitoring permafrost environments, case study from Herschel Island, Canada *Remote Sens. Environ.* **115** 3491–506
- Smith S L *et al* 2010 Thermal state of permafrost in North America: a contribution to the International Polar Year *Permafrost Periglac. Process.* **21** 117–35
- Snyder N P 2009 Studying stream morphology with airborne laser elevation data *EOS Trans. AGU* **90** 45–6
- Streletskiy D A, Shiklomanov N I, Nelson F E and Klene A E 2008 Thirteen years of observations at Alaskan CALM sites: long-term active layer and ground surface temperature trends *9th Int. Conf. on Permafrost Fairbanks* ed D L Kane and K M Hinkel pp 1727–32
- Stroeve J C, Serreze M C, Holland M M, Kay J E, Malanik J and Barrett A P 2012 The Arctic's rapidly shrinking sea ice cover: a research synthesis *Clim. Change* **110** 1005–27
- Sultan N J, Braun K W and Thieman D S 2011 North Slope trends in sea level, storm frequency, duration and intensity *Ice Tech Conf. Prudhoe Bay Paper No. ICETECH10-155-R0*
- Walker D A *et al* 2008 Patterned-ground ecosystems: a synthesis of field studies and models along a North American Arctic Transect *J. Geophys. Res.* **113** G03S01
- White S A and Wang Y 2003 Utilizing DEMs derived from LIDAR data to analyze morphologic change in the North Carolina coastline *Remote Sens. Environ.* **85** 39–47
- Woolard J W and Colby J D 2002 Spatial characterization, resolution, and volumetric change of coastal dunes using airborne LIDAR: Cape Hatteras, North Carolina *Geomorphology* **48** 269–87